Dynamic Effects for Two-Phase Flow in Porous Media: Fluid Property Effects

Diganta Bhusan Das, Robert Gauldie, and Mahsanam Mirzaei
Dept. of Engineering Science, The University of Oxford, Oxford OX1 3PJ, U.K.

DOI 10.1002/aic.11292
Published online August 30, 2007 in Wiley InterScience (www.interscience.wiley.com).

Traditional descriptions of multiphase flow in porous media rely on an extension of Darcy's law along with relationships between capillary pressure (P^c)*, saturation* (S)*, and relative permeability* (K_r)*. New theories have been proposed which suggest that* P^c *relationships should include a dynamic coefficient* (τ) *(Hassanizadeh and Gray,* Water Resour Res. *1993;29:3389–3405) to indicate how "quickly" or "slowly" flow equilibrium is reached. While validity of these theories must be examined, it is also necessary to determine the significance of* τ *and its range of values. In this article, we analyze the significance of* τ *depending on fluid properties. We address the ways in which they cause nonuniqueness of dynamic two-phase flow in porous media and, hence, dynamic effect. Simulations are conducted for quasi-static and dynamic flow of perchloroethylene (PCE) in water saturated domains. The data are then fitted to the dynamic* P^c *relationships to obtain values of* τ*. The effects of flow directions and, viscosity and density ratios are discussed. To consider the lumped effects of various fluid properties,* τ–S *relationships are examined for silicone oils. The results are interpreted by examining the correlation between* τ *and a mobility coefficient,* m*. We discuss a scaling relationship that shows the dependence of* τ *on fluid and material properties.* © 2007 American Institute of Chemical Engineers *AIChE J,* 53: 2505–2520, 2007

Keywords: two-phase flow, porous medium, capillary pressure, relative permeability, saturation, dynamic effect, nonaqueous phase liquids, fluid property, scaling relations

Introduction

The displacement of one or more fluid(s) by other immiscible fluid(s) in porous media is encountered in many chemical, petroleum, and environmental engineering problems. A common example is the subsurface contamination by nonaqueous phase liquids, NAPLs (e.g., oils, perchloroethylene (PCE), etc), produced and accidentally spilt by various chemical process industries. They may remain in the subsurface for hundreds of years and are an environmental threat worldwide. Current approaches for describing immiscible flow behavior at continuum scale are based on a multiphase version of Darcy's law and, constitutive relationships between capillary pressure (P^c), saturation (S), and relative permeability (K_r), which are generally obtained at quasi-static conditions.[3–7] The P^c–S–K_r relationships are highly nonlinear in nature and depend on a number of factors, e.g., flow dynamics (i.e., steady or dynamic), dominant forces (e.g., capillary or viscous), contact angles, material properties, types of heterogeneity, boundary conditions, scales of observation, etc. Effects of these parameters have been discussed extensively in the above literature and others.[8–14] The main focus of discussion in this article is the relationships between fluid properties (e.g., viscosity and density ratio) and dynamic effects in P^c–S–K_r relationships for two-phase flow in 3D porous media.

One of the most controversial issues in the current theories of multiphase flow in porous media, which has received con-

Correspondence concerning this article should be addressed to D. B. Das at this current address: Dept. of Chemical Engineering, Loughborough University, Loughborough LE11 3TU, UK; e-mail: D.B.Das@Lboro.ac.uk.

siderable attention in the literature, is the significance and interpretation of dynamic capillary pressure effects on multiphase flow behavior.[1,2,9,15–20] This is different from the effects of dynamic flow rate at domain boundaries and, can be defined as the dependence of P^c–S–K_r relationships on time derivative of saturation ($\partial S/\partial t$) while the fluid flow at domain boundary may or may not be time dependent. The "dynamic capillary pressure" effect, to be called as "dynamic" or "nonequilibrium" effect from here after, stems from the fact that at the pore scale the fluid–fluid interfaces have a tendency to change positions so that the multiphase system obtains an equilibrium between external and internal forces governing the flow dynamics and, hence, $\partial S/\partial t$.[21] If the governing forces change in magnitude from equilibrium values, the fluid–fluid interfaces tend to move to new equilibrium positions. Over the years, a number of approaches have been reported which attempt to describe how fluid phases or fluid–fluid interfaces move in porous materials under nonequilibrium conditions.[22–24] It is accepted that when a multiphase system reaches equilibrium the fluid phases maintain own flow paths through the domain.[25] However, to reach equilibrium positions the fluid phases need a finite relaxation time depending on the scales of observation and any other conditions.[2,21] This is generally characterised by a "capillary damping coefficient" or "dynamic coefficient" or "relaxation parameter," which determines the speed and/or the ease with which flow equilibrium is reached. For example, in porous domains with micro-heterogeneities, the fluid–fluid interfaces need larger relaxation time or force/energy to reach equilibrium positions. Hence, the dynamic coefficients are higher in heterogeneous porous domains as compared with those in homogeneous domains.[2]

If the steady state P^c–S–K_r relationships are employed to describe a dynamic two-phase flow system, as commonly done, it implies that any disturbance in the system due to changes in governing forces is eliminated instantaneously or within a short period of time. This is plausible in some cases, e.g., if the domain is very small in size. However, in most realistic cases, the above assumption is contrary to experimental and theoretical evidence, as discussed in a number of previous studies.[2,15,19,20] In general, the P^c–S–K_r relationships need many days to weeks to reach equilibrium at laboratory scale domains (10- to 12-cm long). For larger scale problems or low permeability materials, this time period is envisaged to be even bigger. For the P^c relationships to be independent of dynamic effects so that the current multiphase flow theories based on steady state assumptions may be used at shorter time durations, the system must be independent of flow dynamics. Since this is not the case, Hassanizadeh and Gray[1] proposed a capillary pressure relationship which relates average P^c at dynamic ($P^{c,dyn}$) and equilibrium ($P^{c,equ}$) conditions and, include a damping coefficient (τ), as shown below:

$$\left(P^{c,dyn} - P^{c,equ}\right)|_S = -\tau \frac{\partial S}{\partial t}|_S \qquad (1)$$

where S is the average water saturation [−] in the domain and, t is the time [s]. In Eq. 1, the capillary pressure, P^c [kgm^{-1} s^{-2}], is defined as $(P_{nw} - P_w)$ for both equilibrium ("equ") and dynamic ("dyn") flow conditions, where P_{nw} and P_w are the average pressure [kgm^{-1} s^{-2}] of the nonwetting and wetting fluid phases, respectively. τ [kgm^{-1} s^{-1}] establishes the speed at which fluid–fluid interfaces reach equilibrium positions and, provides a linear dependence of $\left(P^{c,dyn} - P^{c,equ}\right)$ on $\partial S/\partial t$. While the qualitative meaning of τ is understood, there are still significant uncertainties on the range of its values for various cases and hence applying Eq. 1 to solve real life problems. In very small domains, where the fluid–fluid interfaces may reach equilibrium instantaneously, one may argue that $\tau \cong 0$. In these cases, Eq. 1 reduces to $P^{c,dyn}|_S \cong P^{c,equ}|_S$, which means that the dynamic and steady state P^c are the same at that scale at a given saturation. However, if the domain size increases τ also increases implying that the relaxation time for the fluid–fluid interfaces is higher. This was discussed by Gielen et al.[16] who reported a dynamic pore scale network model and showed that τ increases with increasing averaging domain size. Gielen et al.[16] reported values of τ up to 1.2×10^5 kgm^{-1} s^{-1}.

In general, any parameter that increases the relaxation time for the fluid–fluid interfaces also increases the value of τ, or vice versa. Mirzaei and Das[2] examined the effects of porous media permeability on τ in 3D core scale domains (with gravity effect) and showed that τ is higher for a domain with lower permeability. Bourgeat and Panfilov[9] rightly argued that nonequilibrium effects are caused by heterogeneity in porous media. Hassanizadeh et al.[15] used a number of data sets from the literature to demonstrate that dynamic effects exist in laboratory scale experiments for measuring P^c–S–K_r relationships, which are in the range 3.0×10^4 to 2.0×10^7 kgm^{-1} s^{-1}. Manthey et al.[18] carried out simulations of 2D drainage experiments (without gravity) to investigate effects of micro-heterogeneities on τ and reported values between 10^3 and 10^7 kgm^{-1} s^{-1}. Mirzaei and Das[2] also examined the micro-heterogeneity effects on τ in 3D core scale domains (with gravity) and showed that τ increases with the amount of heterogeneity in the domain provided the heterogeneities are fine material (less permeable) imbedded in coarser material (more permeable). They showed that τ is a nonlinear function of water saturation and it increases as wetting phase saturation decreases. The studies by Bourgeat and Panfilov[9], Manthey et al.,[18] and Mirzaei and Das[2] are particularly important since real porous samples (e.g., soil) invariably contain regions of heterogeneity and/or areas of varying permeability. Mirzaei and Das[2] also carried out numerical experiments in both 2D and 3D cylindrical homogeneous and heterogeneous domains and reported values of the order of 10^5 to 10^9 kgm^{-1} s^{-1}. Mirzaei and Das indicated that τ is almost the same in 2D or 3D homogeneous domains for isotropic permeability whilst it is generally higher for 3D heterogeneous domain as compared to those for 2D heterogeneous domain for the same intensity of heterogeneity. τ is also shown to increase with decrease in permeability anisotropy ratio, defined as the ratio of the vertical permeability to horizontal permeability. Oung et al.[20] examined centrifugally accelerated drainage and imbibition with water and PCE and, pointed out that the results obtained from such experiments do not represent static flow conditions due to nonequilibrium effects. They calculated τ at higher water saturation ($S \geq 0.5$) in the range of 90 to 270 kgm^{-1} s^{-1} for fine sand and 14 to 55 kgm^{-1} s^{-1} for coarse sand.

At first sight it may seem that the above observations are general enough that they may hold for any combination of

wetting and nonwetting fluids. However, this is not the case and the roles of fluid and material properties and, the interplay of various forces that determine equilibrium behavior of multiphase systems are very complex. Consider, for example, the frontal instabilities of fluid–fluid interfaces, which depend strongly on fluid properties along with the domain microstructural characteristics. These instabilities affect the dynamics of the multiphase systems and may generate viscous or gravity fingers of various shapes and sizes. At the moment, there is little work in the open literature, which considers the changes in dynamic coefficient (τ) due to variation in fluid properties in realistic cases, e.g., 3D domain with gravity forces, and therefore it is difficult to draw any general conclusion(s) as to the effects of fluid properties on τ.

Stauffer[8] came up with the following scaling relationship from laboratory experiments of unsaturated flow, which gives a dependence of the relaxation parameter on various material and fluid properties:

$$\tau = \frac{\alpha\phi\mu}{\lambda K}\left(\frac{P^{\mathrm{d}}}{\rho g}\right)^2 \tag{2}$$

where τ is the relaxation parameter, α is a dimensionless parameter (defined to be 0.1); ϕ and K are the porosity and intrinsic permeability of the material (isotropic); μ and ρ are the viscosity and density of the wetting phase; P^{d} and λ are the Brooks and Corey parameters which depend mainly on the pore and particle size distribution of the materials and, g is the gravity constant. Stauffer showed that the relationship between $\frac{P^{\mathrm{c,dyn}}-P^{\mathrm{c,equ}}}{\rho g}$ and $\phi\frac{\partial S}{\partial t}$ is a straight line. Hassanizadeh et al.[15] substituted various $\hat{\tau}\left(=\frac{\tau}{\phi\rho g}\right)$ into a numerical model based on dynamic capillary pressure relationships to determine the range of $\hat{\tau}$ that has a tangible effect (>10%) on unsaturated flow behavior and obtained values of $\hat{\tau} > 10^6$. Tsakiroglou et al.[26] performed drainage experiments with paraffin oil and water in a 2D horizontal etched glass pore scale network. Tsakiroglou et al. concluded that at the pore scale the displacement of fluids is capillary force dominated. On the other hand, at the network scale, the fluid displacement is dominated by capillary or viscous forces depending on the size of the network and capillary number (Ca). They define Ca as the ratio of the pressure drop across a single pore to the capillary pressure required for filling a pore with nonwetting fluid. Tsakiroglou et al. reported values of τ in the range 10^6–10^8 kgm^{-1} s^{-1}. By using a bundle of noninteracting capillary tube model of different pore size distributions, Dahle et al.[17] showed that the value of the dimensionless group $\tau K/\phi\mu L^2$ increases with decrease in the wetting phase saturation (S), except at high saturation ($S \geq 0.8$) where this trend is the opposite. In this dimensionless group, L is a characteristic length of the domain. Recently, Gielen[27] has considered effects of viscosity ratios on τ using a pore scale network model for cases where (a) effects of gravity are ignored and (b) domain size is much smaller compared with the one used in this article. Gielen reports maximum τ values of ~4000 kgm^{-1} s^{-1} for viscosity ratio ($\mu_{\mathrm{nw}}/\mu_{\mathrm{w}}$) of 20 at wetting phase saturation 0.4. Gielen also finds that τ increases with increase in viscosity ratio, i.e., as the stability of fluid fronts increase. We show later in this article that the opposite trend may be found, i.e., τ values decrease with increase in the stability of fluid fronts.

The above studies clearly show the importance of considering the effects of fluid properties on τ. As mentioned before, the interplay of various forces and fluid properties, which determine τ for given material properties and domain size, is such that they need careful considerations. If the scenario is such that the fluid–fluid interfaces are unstable at a given saturation, then one may envisage that τ would be higher compared with another case at the same saturation where the interfaces are more stable. However, whether or not this hypothesis is correct needs a thorough analysis. The spatial and temporal distributions of the fluid–fluid interfaces affect the average fluid saturation (S) in the domain. However, they are of less importance in the present context as we are interested in determining macroscopic τ–S relationships and not (i) the distribution of the dynamic fluid/fluid interfaces and (ii) the size and shape of the fingers that may generate in the domain. In fact, we recognise that it is not trivial to relate the effects of (i) and (ii) on τ using the continuum scale modelling tool used in this study. Other approaches have been reported which consider the dynamics of fluid–fluid interfaces[22–24,26,28] and development of fingers for both saturated and unsaturated porous domain,[29] which the readers may refer to, if interested.

Following the above discussions, this work aims to characterize dynamic capillary pressure effects on two-phase flow in porous media by examining the variation of the capillary damping coefficient (τ) for a number of numerical drainage experiments at the core scale. Our main objective is to address the effects of viscosity and density ratios of the fluid phases on τ. The importance of gravity forces in causing dynamic effect is considered by simulating two-phase fluid flow in various directions. To aid in our analysis, a simple criterion is developed (Appendix 1), which allows determining whether the fluid front is less or more stable depending on fluid properties, directions of flow, etc. The concluding section summarises the findings in this work and also discusses a functional relationship, which shows the dependence of τ on various fluids and material properties.

Governing Model Equations

In this section, we discuss the model equations used to describe two-phase flow behavior in porous media.

Mass balance

Conservation of fluid mass in the porous media is governed by the following continuity equation,

$$\frac{\partial}{\partial t}(\phi\rho_\alpha S_\alpha) + \nabla\left(\rho_\alpha \overline{Q}_\alpha\right) = 0 \quad \text{for} \quad \alpha = \mathrm{w}, \mathrm{nw} \tag{3}$$

where ϕ [−] is the porous media porosity, $\overline{Q}_\alpha$ [m^3 s^{-1}] is the average flux, S_α [−] is the saturation, and ρ_α [kgm^{-3}] is the density of fluid phase α. As evident, the conservation equation is written in terms of fluid saturation (S_α) in the domain which is the ratio of the volume of fluid phase α in the sample to the total pore volume of the sample. The saturation of the wetting (w) and nonwetting (nw) phases in the domain are related as below,

$$S_{\mathrm{w}} + S_{\mathrm{nw}} = 1 \tag{4}$$

Force balance

Multiphase flow through porous media is the result of gravity, viscous, pressure, and inertia forces although for most practical cases inertial forces can be neglected. In this work, the multiphase version of Darcy's equation is used to describe the conservation of forces for wetting (w) and non-wetting (nw) phases:

$$\overline{Q}_\alpha = -\frac{K_{r\alpha}K}{\mu_\alpha}(\nabla P_\alpha + \rho_\alpha g \nabla \mathrm{z}) \quad \text{for} \quad \alpha = \mathrm{w}, \mathrm{nw} \tag{5}$$

where, $\overline{Q}_\alpha$ [$m^3\ s^{-1}$] is the average Darcy flux, K [m^2] is intrinsic permeability defined as isotropic in this work, $K_{r\alpha}$ [$-$] is relative permeability, μ_α [$kgm^{-1}\ s^{-1}$] is dynamic viscosity, ∇P_α [$Kgm^{-2}\ s^{-2}$] is pressure gradient of phase α, and ∇z [$-$] is the gradient of upward unit vector.

Brooks–Corey relationship for capillary pressure

Brooks and Corey[4] relationship is used in this work to relate capillary pressure to wetting phase saturation,

$$S_{\mathrm{ew}} = \left(\frac{P^{\mathrm{c}}}{P^{\mathrm{d}}}\right)^{-\lambda} \quad \text{for} \quad P^{\mathrm{c}} \geq P^{\mathrm{d}} \tag{6}$$

$$S_{\mathrm{ew}} = 1 \quad \text{for} \quad P^{\mathrm{c}} < P^{\mathrm{d}} \tag{7}$$

$$S_{\mathrm{ew}} = \left(\frac{S_{\mathrm{w}} - S_{\mathrm{rw}}}{1 - S_{\mathrm{rw}}}\right) \quad \text{for} \quad 0 \leq S_{\mathrm{ew}} \leq 1 \tag{8}$$

where, S_{ew} [$-$] is the effective wetting phase saturation, P^{d} [Nm^{-2}] is entry pressure, λ [$-$] is pore size distribution index and S_{rw} [$-$] is irreducible wetting phase saturation.

Brooks–Corey–Burdine relationship for relative permeability

The presence of two or more fluid phases affects the permeability of the media to each fluid phase. Pore space available to a phase for flow is decreased by the presence of other phase(s) and, the length and tortuosity of the flow paths increased. There are also viscous interactions between the two fluids at the interface between them, which affect the permeability of the fluid. To include these processes in the simulation of two-phase flow, we use the Brooks–Corey–Burdine[4] relationship, which allows the calculation of relative permeability for each phase in porous media.

$$K_{\mathrm{rw}} = S_{\mathrm{ew}}\left(\frac{2+\lambda}{\lambda}\right) \tag{9}$$

$$K_{\mathrm{rnw}} = (1 - S_{\mathrm{ew}})^2\left(1 - S_{\mathrm{ew}}\left(\frac{2+\lambda}{\lambda}\right)\right) \tag{10}$$

where, the relative permeability, K_{rw} and K_{rnw}, of the wetting and non-wetting phases in the domain.

Averaging procedures

To determine the average capillary pressure for the domain we use a saturation weighted capillary pressure at each numerical node, as shown in Eq. 11:

Saturation weighted average P^{c}:

$$P^{\mathrm{c}}|_{t_n} = \langle P_{\mathrm{nw}}\rangle|_{t_n} - \langle P_{\mathrm{w}}\rangle|_{t_n} = \left(\frac{\sum_{\mathrm{j}=1}^{\mathrm{m}}(1 - S_{\mathrm{wj}})P_{\mathrm{nwj}}}{\sum_{\mathrm{j}=1}^{\mathrm{m}}(1 - S_{\mathrm{wj}})} - \frac{\sum_{\mathrm{j}=1}^{\mathrm{m}} S_{\mathrm{wj}}P_{\mathrm{wj}}}{\sum_{\mathrm{j}=1}^{\mathrm{m}} S_{\mathrm{wj}}}\right)\Bigg|_{t_n} \tag{11}$$

where t_n [s] is an arbitrary n^{th} time step, $\langle P_{\mathrm{nw}}\rangle|_{t_n}$ and $\langle P_{\mathrm{w}}\rangle|_{t_n}$ [Nm^{-2}] are the volume averaged nonwetting and wetting phase pressure, P_{nwj} and P_{wj} [Nm^{-2}] are the nonwetting and wetting phase pressures, and S_{nwj} and S_{wj} [$-$] are the saturation corresponding to nonwetting or wetting phase pressure at time t_n in an arbitrary j^{th} node, where j = 1, 2, 3, . . . , m, m being the total number of nodes in the domain.

At individual node, the saturation and volume of the wetting and nonwetting fluids are related as below,

$$V_{\mathrm{wj}} + V_{\mathrm{nwj}} = \phi \times V_{\mathrm{j}} \tag{12}$$

$$S_\varepsilon = \frac{V_{\alpha\mathrm{j}}}{V_{\mathrm{j}} \times \phi}, \quad \alpha \equiv w, nw \tag{13}$$

$$S_{\mathrm{wj}} + S_{\mathrm{nwj}} = 1 \tag{14}$$

where V_{wj}, V_{nwj} are the volumes of wetting and nonwetting fluid phases in the 3D cell centred around an the arbitrary node j of volume V_{j}, respectively. S_{nwj} is the saturation of the nonwetting phase at node j.

We use a volume averaging of water saturation to calculate the average water saturation in the domain at different times.

Volume averaged water saturation:

$$S_{\mathrm{w}}|_{t_n} = \frac{\sum_{\mathrm{j}=1}^{\mathrm{m}} S_{\mathrm{wj}}V_{\mathrm{j}}\big|_{t_n}}{\sum_{\mathrm{j}=1}^{\mathrm{m}} V_{\mathrm{j}}} \tag{15}$$

We also need values of $\partial \mathrm{S}/\partial \mathrm{t}$ at a specific saturation and time to estimate τ as discussed in the section titled "determination of dynamic coefficient (τ)." This is calculated by a linear interpolation between the values of $\partial \mathrm{S}/\partial \mathrm{t}$ at neighbouring points on S–t curve, as shown below:

$$\left.\frac{\partial S}{\partial t}\right|_{S,t_n} = \frac{1}{2}\left(\frac{S_{\mathrm{w}}|_{t_n} - S_{\mathrm{w}}|_{t_{n-1}}}{t_n - t_{n-1}} + \frac{S_{\mathrm{w}}\big|_{t_{n+1}} - S_{\mathrm{w}}|_{t_n}}{t_{n+1} - t_n}\right) \tag{16}$$

where $S_{\mathrm{w}}|_{t_{n-1}}$, $S_{\mathrm{w}}|_{t_n}$, $S_{\mathrm{w}}\big|_{t_{n+1}}$ are the average saturation in the domain are corresponding to time t_{n-1}, t_n, t_{n+1}.

Description of Numerical Simulation

Simulator used: Subsurface Transport Over Multiple Phases

The two-phase flow simulations have been carried out using the oil–water mode of STOMP (http://stomp.pnl.gov/).[30]

STOMP is a FORTRAN code which was developed to simulate various modes of two-phase flow phenomena. It has

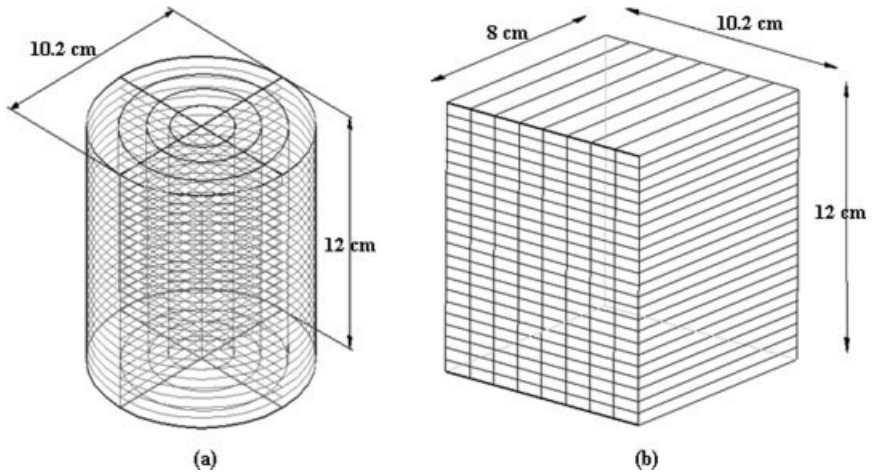

Figure 1. (a) 3D cylindrical porous domain (b) 2D rectangular domain on *x–z* plane of a 3D rectangular domain.

The 3D cylinder is used in most simulations while the 2D domain is used to investigate the effects of flow directions on the dynamic coefficient (τ). The volumes of the 3D and 2D domains are almost the same. Further, the area of the 2D plane is the same as the 2D plane passing through the middle of 3D domain in (a). The effects of domain shapes on τ are discussed by Mirzaei and Das.[2]

been applied to a number of engineering problems including study of dynamic capillary pressure effects.[2,13,14,31–33] The spatial discretisation of the governing equations is done using a standard finite volume method.[34,35] This ensures that mass is conserved in individual numerical cells as well as the entire domain. The nonlinear terms in the discretized governing equations are linearized using the Newton–Raphson iterative method for multiple variables. Temporal discretization is based upon an implicit time stepping. Numerical results are shown to have negligible dependence on the mesh size.[2,13,14] Operation of the simulator relies on a series of input cards in which the geometry of the domain, boundary conditions, fluid and material properties, constitutive relationship, convergence criteria, etc., are specified.

Model parameters

Figures 1a,b shows the dimensions and spatial discretization of the domains used. In most simulations in this work, we use the three dimensional (3D) cylindrical domain (Figure 1a). However, a two dimensional (2D) rectangular plane/domain of a 3D rectangle (Figure 1b) is also used in this work to investigate the effects of flow direction and gravity on dynamic coefficient. The model parameters used in our simulations are detailed in Tables 1 and 2. We have chosen the same parameters as used by Das et al.[13,14] and Mirzaei and Das[2] to maintain a continuity of our previous work. In most cases, we have used PCE and water as the nonwetting and wetting fluid (Table 2) at a reference temperature of 20°C. However, in some cases, we have also used silicone oils and water as the nonwetting and wetting phase (Table 2) at reference temperature of 25°C. Two different reference temperatures are chosen because PCE properties are available at 20°C while properties of silicone oil are available at 25°C. In Table 3, the number of cells and nodal spacing for 2D rectangular and 3D cylindrical domains are shown, corresponding to Figures 1a,b.

Table 1. Porous Media Properties Used in Our Simulations[2,13,14,33,36]

Property	Coarse Sand	Fine Sand
Permeability, $K(\mathrm{m}^2)$	5×10^{-9}	5×10^{-12}
Porosity, $\phi(-)$	0.40	0.40
Displacement pressure, $P^{\mathrm{d}}(\mathrm{kgm}^{-1}\ \mathrm{s}^{-2})$	370	1325
Pore size distribution index, $\lambda(-)$	3.86	2.49
Irreducible water saturation, $S_{\mathrm{iw}}(-)$	0.078	0.098

Initial and boundary conditions and determination of capillary pressure relationships

We have carried out the simulations to mimic pressure cells for the measurement of drainage P^{c}–S–K_{r} relationships. The domain is defined to be fully saturated with water (wetting phase) initially. Then, the nonwetting phase is forced into the domain which drains water out of the porous sample. We impose "no-flow" boundary conditions for the wetting and nonwetting phases on the inflow and outflow faces, respectively. The side walls of the domain are defined to be impermeable to both fluid phases. The boundary conditions used for the dynamic simulations are shown in Table 4. For both steady-state and dynamic simulations the wetting phase on the outflow face is held at atmospheric pressure.

In all simulations, the domain is defined to be a homogeneous porous sample. The procedures to determine the quasi-static P^{c} relationships are as follows. An arbitrary but extremely small initial pressure of nonwetting phase is defined. A zero initial pressure is not imposed to avoid numerical errors in the simulations. Then, the pressure of the nonwetting phase on the boundary of injection is gradually increased. When P^{c} is the same as the entry pressure (P^{d}) of the medium, nonwetting phase enters the sample and displaces water. The simulation is carried out until steady-state flow conditions are reached according to the imposed tolerance limit, that is, saturation at all grid points does not change with time or $\partial S/\partial t$ is smaller than a tolerance limit (10^{-10} in this case). The calculated average saturation and P^{c}

Table 2. Properties of Fluids Used in This Work: Water, PCE, and Silicone Oils (Oil 1–4)

Fluid	Reference Temperature (°C)	Absolute Viscosity μ (cP)	Viscosity Ratio at Reference Temperature $v = \mu_{nw}/\mu_w$ (−)	Specfic Gravity (−)	Surface Tension (dynes/cm)
Water	20	1.0	–	1.002	35.0*
Water	25	0.891	–	1.000	72.0†
PCE	20	0.9	0.9	1.630	21.1*
Oil 1‡	25	0.493	0.6	0.760	15.9*
Oil 2‡	25	4.58	5.1	0.916	19.7*
Oil 3‡	25	48.05	54.0	0.963	20.8*
Oil 4‡	25	485.53	545.0	0.973	21.1*

*Water–PCE/Oil system.
†Water–air system.
‡Reference: www.baschem.co.uk.

provide one point of the P^c–S curve. This is the point where fluid phases moves to equilibrium positions such that the imposed forces are the same as forces within the domain. The imposed nonwetting phase pressure is then increased and the simulation is continued until a new steady state is obtained. This provides a second point for P^c–S curve. The same procedure is continued until a P^c of 11,000 Pa is reached. At this point the sample is deemed to have reached its irreducible wetting phase saturation (S_{rw}). In Figure 2, we show how a single point on a steady-state P^c–S curve is derived from the simulated data. In the figure, the dashed line is the imposed boundary P^c at different time intervals while the full lines are the domain averaged data as it reaches steady state. For simulating dynamic two-phase flow behavior, the imposed nonwetting phase pressure at the top of domain is increased to a high pressure once and drainage is allowed to take place until the domain reaches S_{rw}.

Determination of dynamic coefficient (τ)

To determine the dynamic coefficient (τ), the P^c–S curves obtained from quasi-static and dynamic simulations are used. The average values of $P^{c,dyn}$, $P^{c,equ}$ and $\partial S/\partial t$ are determined as described in the section titled averaging procedure. The averaged data for $\left(P^{c,dyn} - P^{c,equ}\right)$ and $\partial S/\partial t$ are then fitted to a straight line, if possible. The slope of this straight line provides the dynamic coefficient (τ) for that particular case. This is in accordance with Eq. 1 which shows that if $P^{c,dyn}$, $P^{c,equ}$ and time derivative of saturation ($\partial S/\partial t$) are known at a given saturation value, τ can be determined.

Results and Discussions

A number of authors have discussed various features of dynamic and static P^c–S–K_r curves for different cases.[2,10,14,15,19,27] Nevertheless, we present some typical P^c–S curves for drainage of water by PCE in a 3D fine sand domain for completeness of the discussion in this article (Figures 3 and 4). As discussed before, the simulated data are fitted to the linear dynamic P^c relationship (Eq. 1) and τ calculated following the procedures discussed in section "determination of dynamic coefficient (τ)." It is obvious from our results (Figure 5) that the data fit reasonably well to the relationship for $S_w < 0.4$ if an additional intercept parameter "b" is included although no obvious correlation between "b" and the model parameters are found. When $S_w > 0.4$, our results do not conform to the linear relationship accurately and τ values are relatively small ($\tau < 10^6$ kgm^{-1} s^{-1}). This is observed for both fine and coarse sand domains for the properties mentioned in Table 1. At $\tau > 10^5$ kgm^{-1} s^{-1} the dynamic effect, i.e.,$\left(P^{c,dyn} - P^{c,equ}\right)$, becomes appreciable for both coarse and fine sand for the parameters and domain size chosen in this work. We also observe that at higher wetting phase saturation, the linear relationship may not be the most appropriate functional form to fit the simulated data.

Consistent with most previous studies, τ is found to increase with decrease in aqueous saturation and it becomes particularly large for low aqueous saturations (Figure 5). Here $\partial S/\partial t$ is small and the equilibrium conditions are approached slowly, perhaps due to disconnected fluid phases. At high water saturation when the fluid phases generally remain connected, τ values are found to be smaller, which imply that equilibrium conditions is reached quickly/easily. However this is not the case when water saturation decreases. In this work, dynamic coefficient values up to 10^{11} kgm^{-1} s^{-1} are found close to irreducible water saturation in fine sand (Figure 5). These are larger than most previously reported data in the literature; however it is plausible since most values reported in the literature are for 2D domain without gravity effects, smaller domains and/or at higher aqueous saturation where τ is generally found to be smaller.

Table 3. Number of Nodes and Nodal Spacing for 2D Rectangular and 3D Cylindrical Domain for Download Flow

Domain Geometry	Number of Nodes × Nodal Spacing				
	N × Δr, (cm)	N × ΔΘ, (degree)	N × ΔX, (cm)	N × ΔY, (cm)	N × ΔZ, (cm)
2D Rectangular	–	–	8 × 1.25	1 × 7.92	1 × 0.05, 24 × 0.5, 1 × 0.05
3D Cylindrical	4 × 1.25	4 × 90	–	–	1 × 0.05, 24 × 0.5, 1 × 0.05

N: Number of nodes.
Δ*r*: Nodal Spacing in *r* direction for 3D cylindrical domain.
ΔΘ: Nodal Spacing in Θ direction for 3D cylindrical domain.
Δ*X*: Nodal Spacing in *X* direction for rectangular 2D domain.
Δ*Y*: Nodal Spacing in *Y* direction for rectangular 2D domain.
Δ*Z*: Nodal Spacing in *Z* direction for rectangular 2D domain.

Table 4. Boundary Conditions for Different Dynamic Drainage Cases with NAPL (PCE or Silicone Oil) as Nonwetting Phases

	Inlet Boundary (Top, Left Side or Bottom of Domain)		Outlet Boundary (Bottom, Right Side or Top of Domain)	
Displacement case	Dirichlet NAPL Pressure (Pa)	Zero Flux Water	Dirichlet water Pressure (Pa)	Zero Flux NAPL
Dynamic case-1 50 cm NAPL head	110,505		102,510	
Dynamic case-2 70 cm NAPL head	113,703		102,510	
Dynamic case-3 100 cm NAPL head	118,500		102,510	
Dynamic case-4 135 cm NAPL head	123,297		102,510	

Dirichlet BCs of pressure are imposed for NAPL at the inlet and water at the outlet. Zero flux BCs are imposed for water at the inlet and NAPL at the outlet. The inlet is the top, left side or bottom of the domain depending on whether the flow takes place vertically downward, horizontally or vertically upwards. The outlet is opposite to the inlet face.

Effects of viscosity ratio (μ_{nw}/μ_w) on dynamic coefficient (3D domain)

Our simulations carried out for two-phase flow in fine and coarse sand show that there is no significant variations of τ with viscosity ratio (μ_{nw}/μ_w) below a threshold wetting phase saturation, termed S_v for future reference. In this work $S_v \cong 0.2, 0.27$ for fine and coarse sand as shown in Figures 6 and 7, respectively. We believe this is related to the fact that as wetting phase saturation decreases, the fluid phases get disconnected and/or entrapped in the pore space. Consequently, the viscosity ratio has little role to play in determining the equilibrium behavior of the flow system and, hence, τ.

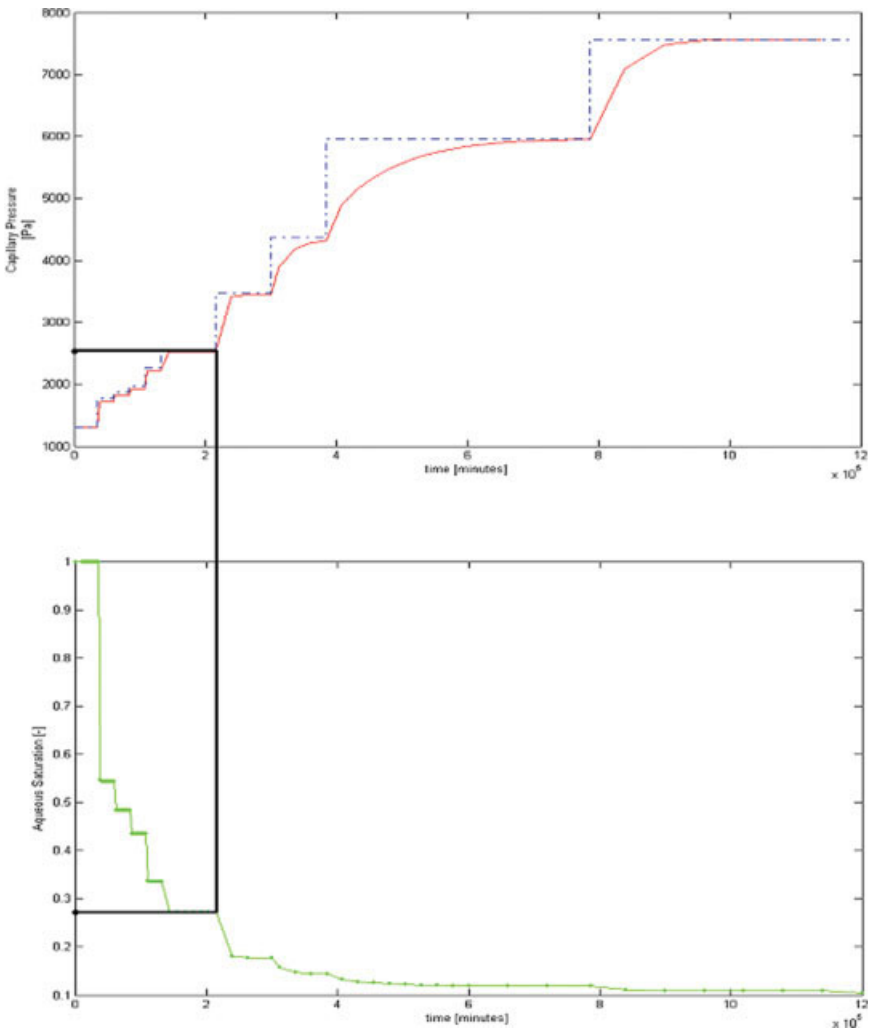

Figure 2. The procedure for deriving a single point on a steady-state P^c–S curve.

The dotted lines are the P^c imposed at domain boundary in this work. The solid lines are the values of P^c or S_w within the domain following Eqs. 11 and 15, respectively. We define equilibrium condition as $\partial S/\partial t \leq 10^{-10}$ while average P^c within the domain is almost equal to the boundary P^c. [Color figure can be viewed in the online issue, which is available at www.interscience.wiley.com.]

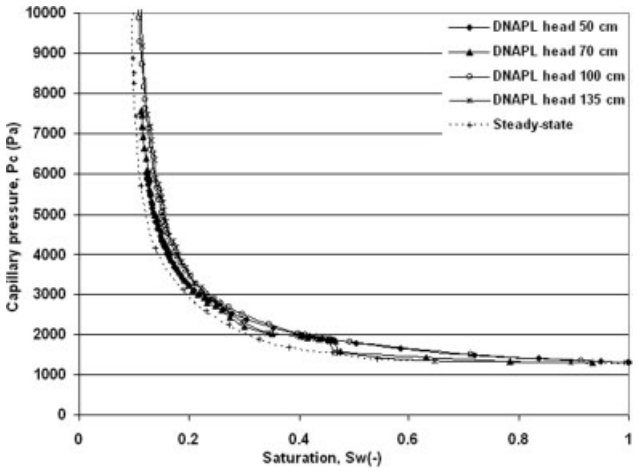

Figure 3. Quasi-static and dynamic drainage P^c–S curves for DNAPL (PCE) flow in fine sand cylindrical domain (3D).

The viscosity ratio is 0.97 for the simulations. Although the P^c–S curves look similar for various DNAPL heads, the time derivative of saturation $(\partial S/\partial t)$ is different in various cases, and hence, the dynamic coefficient (τ).

At higher water saturation, the fluid phases generally remain connected and the viscosity ratio has a more prominent effect on τ. This is confirmed in our results which show that if $S > S_v$, τ generally decreases for a higher viscosity ratio for a given saturation. This implies that τ decreases for increase in DNAPL viscosity. A less viscous invading front advances more quickly into the porous domain. Therefore, it may be tempting to argue that equilibrium conditions are obtained more quickly in this case and hence, τ should be lower for lower nonwetting phase viscosity. However, τ describes the development of equilibrium flow behavior at constant saturation and not time levels. Therefore, this argument is not valid. The stability of the fluid front is the key to determining how quickly this equilibrium is achieved, and hence, the values of τ. To explain this point, we consider a mobility coefficient/ratio (m) defined as,

$$\mathrm{m} = \frac{K_{\mathrm{rw}}\mu_{\mathrm{wn}}}{K_{\mathrm{rnw}}\mu_{\mathrm{w}}} \tag{17}$$

where K_{rw} is the relative permeability of the wetting phase, K_{rnw} is the relative permeability of the nonwetting phase, μ_{nw} is the viscosity of the nonwetting phase and μ_{w} is the viscosity of the wetting phase. In Eq. 17 m, K_{rw} and K_{rnw} are function of average saturation in the domain. Up-scaled K_{rw}–S and K_{rnw}–S relationships are determined from saturation weighted average of local K_{rw}, K_{rnw}, and S_{w} data at each node, for both dynamic and stead-state flow condition.

For the simulations in this section, we maintain the same boundary pressures for the fluid phases but viscosity ratios are changed. However, this also changes the Darcy flux across the domain boundary (Eq. 5) which affects the τ–S relationships. We therefore believe that it is more reasonable to discuss the roles of fluid properties on τ in terms of the mobility coefficient (m) for different viscosity ratios $(\mu_{\mathrm{nw}}/\mu_{\mathrm{w}})$ and not directly with it. This ensures that τ is compared for the same parameter which determines the stability of fluid fronts. As discussed in Appendix 1, the stability of the fluid front is related to the mobility coefficient and not simply the viscosity or density ratios. In general, the fluid front is stable or unstable depending on whether $m > 1$ or $m < 1$, respectively, at a given saturation for drainage of porous material. However, higher is the mobility coefficient, the more stable the fluid front is due to the less time/force/energy required by the multiphase system to establish equilibrium conditions. Therefore, we argue that τ decreases if m increases. This is illustrated in Figure 8 where the corresponding m–S and τ–S relationships for different viscosity ratios are plotted in case of fine sand. The figure shows a clear correlation between m and τ, i.e., as m increases τ decreases at a given saturation. High values of τ are obtained as $S_{\mathrm{w}} \rightarrow S_{\mathrm{irw}}$ because mobility ratio tends to be small. The region of little variation of τ with viscosity ratio (i.e., $S_{\mathrm{w}} < S_{\mathrm{v}}$) also correlates to the region in which m is close to zero.

To calculate the mobility ratios, the K_{r}–S relationships are needed for various viscosity ratios at dynamic conditions. Some typical results are presented in Figure 9 along with the K_{r}–S relationships at quasi-static conditions. Only one quasi-static K_{r}–S curve is shown because changes in the viscosity ratios considered here are found to have practically no effect on the steady-state K_{r}–S curves.

Effects of flow direction on dynamic coefficient (2D and 3D domains)

To synthesise the effects of flow directions on τ–S relationships drainage simulations have been carried for PCE flow (a) downwards from top of the domain (along gravity), (b) upwards from the bottom of the domain (against gravity), and (c) horizontal flow with the domain orientated in the horizontal plane (same gravity effects). To begin with, we have carried out the simulations on 2D rectangular homogeneous domain (Figure 1b) in an attempt to eliminate any effects of dimensionality on τ (Figures 10 and 11). However, we have

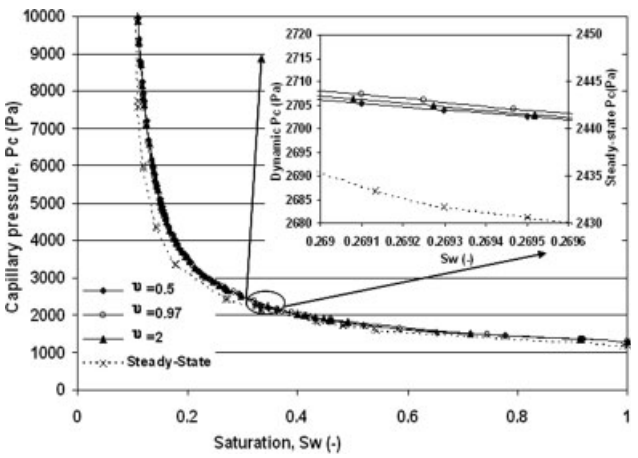

Figure 4. Drainage P^c–S curves (100 cm NAPL head) for varying viscosity ratio (υ) in fine sand cylindrical domain.

The viscosity ratio has practically no effect on quasi-static P^c–S relationships and only one P^c–S curve is plotted.

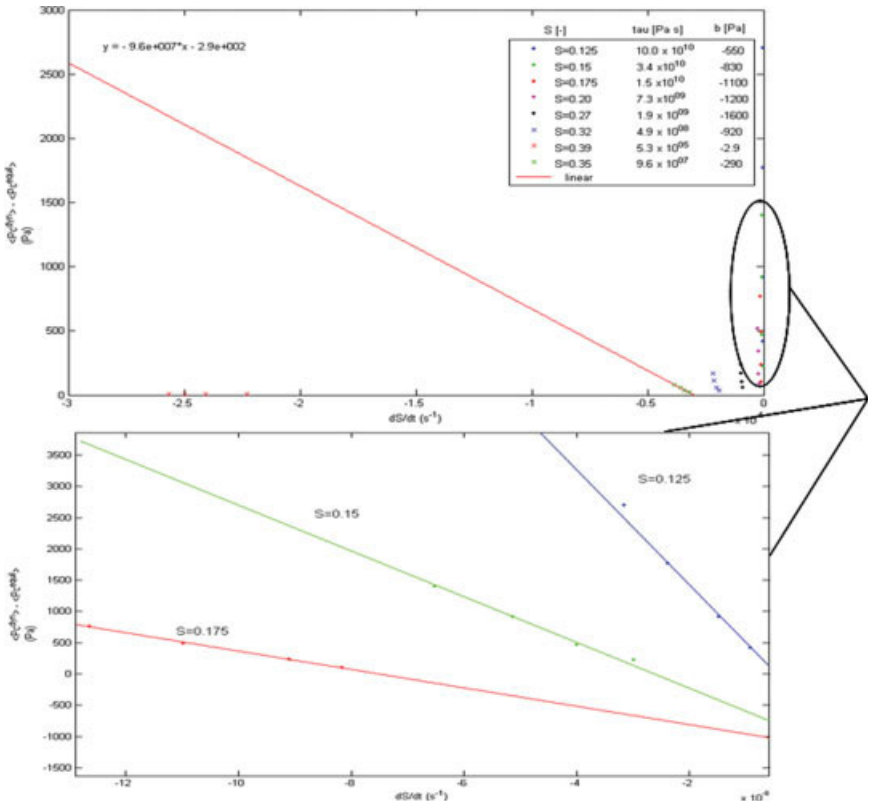

Figure 5. Fitting a linear relationship to the simulated data for capillary damping coefficient determination.

[Color figure can be viewed in the online issue, which is available at www.interscience.wiley.com.]

also determined the τ–S curves for 3D homogeneous sand for cases (a) and (b) in which both effects of flow directions and all three dimensions are present (Figure 12). Our results in Figure 10 show that the highest τ values are obtained for downward infiltration and the lowest for upward infiltration with τ values for horizontal flow in-between. This clearly indicates a directional dependence of the τ–S relationships, which is in keeping with the analysis about stability of the advancing front (Appendix 1). The fluid considered here is a DNAPL where density ratio, $\varsigma(=\rho_{nw}/\rho_w) > 1$ and mobility ratio, $m < 1$ for the saturation range considered. As discussed in Appendix 1, downward flow imparts additional instability to the invading front. Therefore, τ is higher in this case. For flow against gravity, the front is more stable for DNAPL and therefore τ is lower. For horizontal flow, gravity has the same effect on the stability of the fluid front and, therefore, τ values lie between the cases for upward and downward flow. We illustrate this point further in Figure 11 which shows PCE saturation contour plots for the three scenarios at the same average water saturation of 0.3 in the domain. Unstable fronts are not visible for the fluid and material property chosen. However, the varying nature the fronts depending on the infiltration directions at the same mean saturation are evident. A pooling of PCE on the outflow face for all three simulations is seen due to the no flow condition imposed for the nonwetting phase (pressure cell). It seems that for downward flow the front is less stable and a larger

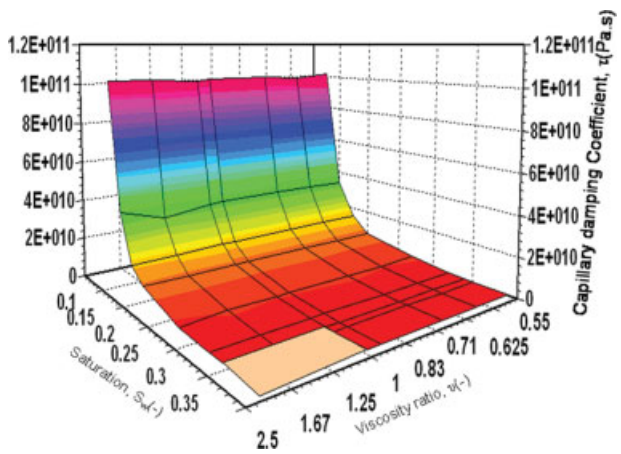

Figure 6. Capillary damping coefficient (τ) for varying viscosity ratio (υ) and aqueous saturation (S_w) in fine sand cylindrical domain (3D).

Note that in the salmon shaded region, approximated values of τ are relatively small and the linear relationship for dynamic capillary pressure is not necessarily the most appropriate form, i.e. it is nonlinear. These points are correct in their order of magnitude but are an approximation due to the fact that we force the data to a linear relationship. [Color figure can be viewed in the online issue, which is available at www.interscience.wiley.com.]

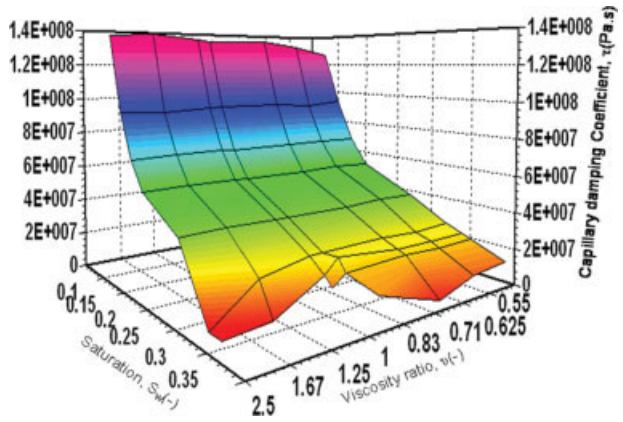

Figure 7. Capillary damping coefficient (τ) for varying viscosity ratio (υ) and aqueous saturation (S_w) in coarse sand cylindrical domain (3D).

[Color figure can be viewed in the online issue, which is available at www.interscience.wiley.com.]

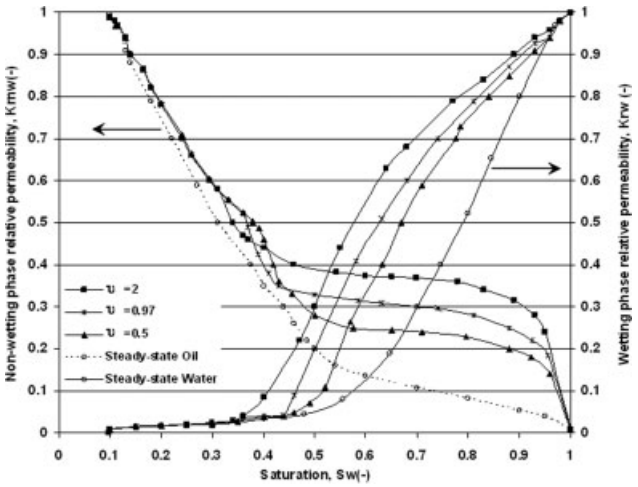

Figure 9. Quasi-static and dynamic (PCE head 100 cm) relative permeability (K_r) of the wetting and nonwetting phases as a function of water saturation for varying viscosity ratio ($\upsilon = \mu_{nw}/\mu_w$).

Viscosity ratio has practically no effect on quasi-static K_r–S relationships and only one curve is plotted in this figure.

amount of PCE accumulates at the outflow face. For upwards flow a smaller amount of PCE accumulates at the outflow face and there is distinctly greater accumulation of PCE nearer to the inflow face for a more stable front. This supports the observation of higher τ value for the case of buoyancy forces in line with flow direction.

In case of 3D domains the effects of flow directions on τ are less prominent (Figure 12), perhaps because the effects of dimensionality are also present. Our drainage simulations suggest that for given fluid properties and boundary conditions, the τ–S relationships are similar for both upward and downward directions; however, in general, τ is higher for downward flow. The same observations are made for various viscosity ratios provided the density ratios are the same, as in the case for Figure 12.

Effects of density ratio (ρ_{nw}/ρ_w) on dynamic coefficient (3D domain)

In this section, we analyze the effects of density ratio ($\varsigma = \rho_{nw}/\rho_w$) on τ. Drainage simulations in a vertical cylindrical domain of fine sand (3D) have been carried out to determine τ–S relationships (Figure 13) for flow downwards from the top of the domain and for flow upwards from the bottom of the domain. The effects of flow directions are particularly important to consider for the density ratio effects although perhaps not so much for the viscosity ratio effects as shown in Figure 12. The nonwetting phase (i.e., PCE) considered here is a DNAPL where density ratio, $\varsigma > 1$ and

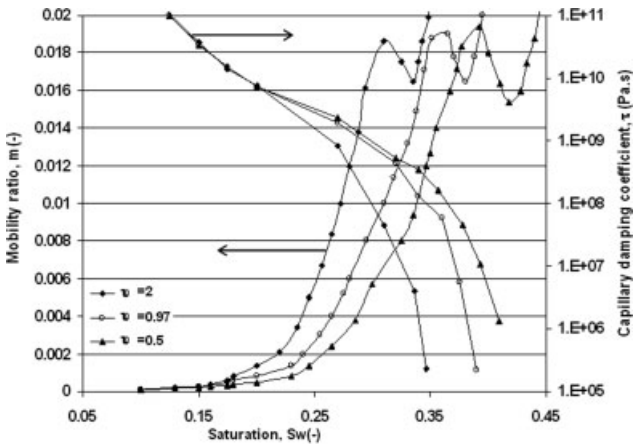

Figure 8. Mobility ratio ($m = K_{nw}\mu_{nw}/K_{rnw}\mu_w$) and capillary damping coefficient (τ) as functions of water saturation (S_w) for varying viscosity ratio ($\upsilon = \mu_{nw}/\mu_w$) in fine sand cylindrical domain (3D).

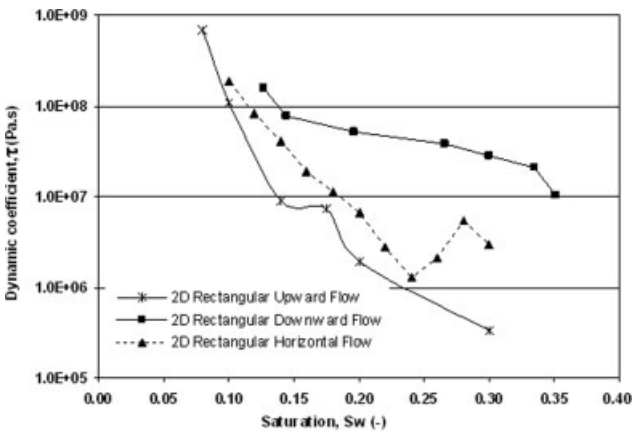

Figure 10. Capillary damping coefficient (τ) for varying flow directions (upward flow against gravity, downward flow along gravity and horizontal with the same gravity effect) in coarse sand rectangular 2D domain.

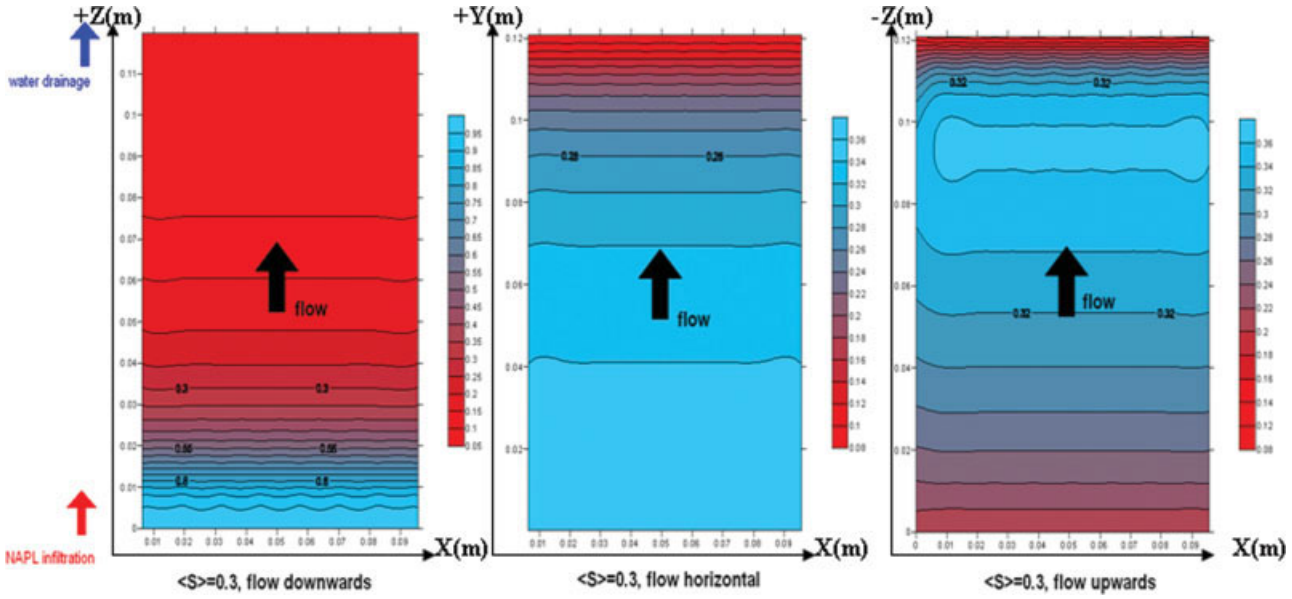

Figure 11. PCE (NAPL) saturation contour plots for varying flow directions in 2D rectangular domains, dynamic head of 100 cm PCE in all cases.

Note that the physical orientation of the domain is as indicated below each domain. The direction of the flow is shown as up the page in all cases to aid the comparison of PCE saturation distribution. [Color figure can be viewed in the online issue, which is available at www.interscience.wiley.com.]

the mobility ratio, $m < 1$ for the saturation range considered. As discussed in Appendix 1, DNAPL imparts additional instability to the invading front for downward flow during drainage and therefore τ is higher in this case. For flow against gravity, the DNAPL front is more stable and therefore τ is generally lower as compared with those for downward flow for given density ratio. As regards to the effects of density ratio in the same flow direction, our results show an increase in τ with increase in density ratio for downward flow (in general). On the other hand, an increase in τ is seen for decrease in density ratio for upward flow. This agrees with the previous observations that buoyancy forces in the direction of flow will impart instability in the advancing front and thus lead to higher τ values. Buoyancy forces opposing flow lead to a more stable fluid front and hence, lower τ values.

Lumped effects of fluid properties on dynamic coefficient (3D domain)

In the previous sections, we have altered either the density or viscosity ratio to determine their effects on the dynamic coefficient keeping all other parameters the same. In practice, however, the fluid propeties are related and, therefore, one should expect a lumped effect of various fluid properties on τ and, not simply the effects of the viscosity, density ratio, or surface tension. To address this issue, we have carried out simulations with silicone oil (polydimethyl-siloxanes) as a model nonwetting fluid for the properties mentioned in Table 2. As shown in the table, silicone oils may have various forms. They are generally lighter than water (i.e., light nonaqueous phase liquid, LNAPL) with similar densities but their viscosities may vary considerably. Therefore, while these fluids allow us determine the lumped effects of fluid properties, in effect, they also enable us to reconfirm our previous observations on the effects of viscosity ratio (μ_{nw}/μ_w) on dynamic coefficient (3D domain) for a wider range of viscosity ratios (0.6–545).

We carry out vertical drainage simulations (along gravity) using the silicon oils (Table 2) as the nonwetting phase in fine sand. The obtained τ–S relationships are as shown in Figure 14. As evident, a trend similar to that found from the simulations for varying viscosity ratio (i.e., Figure 8) is observed. There is slight discrepancy for the lowest viscosity ratio (0.6), as Oil 1 has slightly lower τ values than Oil 2 at low aqueous saturation. This discrepancy is not surprising as Oil 1 has a considerably lower specific gravity and surface tension than the other forms of silicone oils. In general, our results follow the

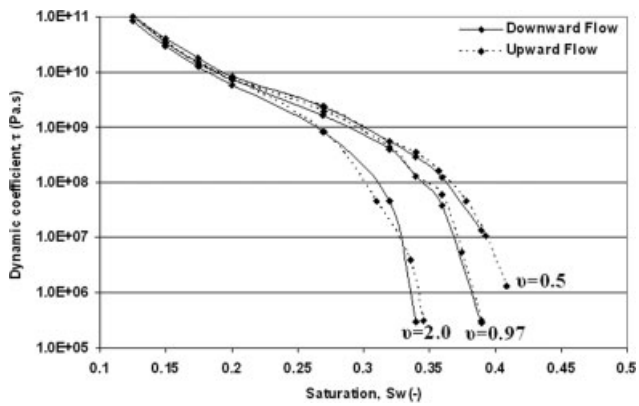

Figure 12. Capillary damping coefficient (τ) for varying viscosity ratio ($\upsilon = \mu_{nw}/\mu_w$) in fine sand cylindrical domain (3D) with flow of PCE downward along gravity and upward against gravity.

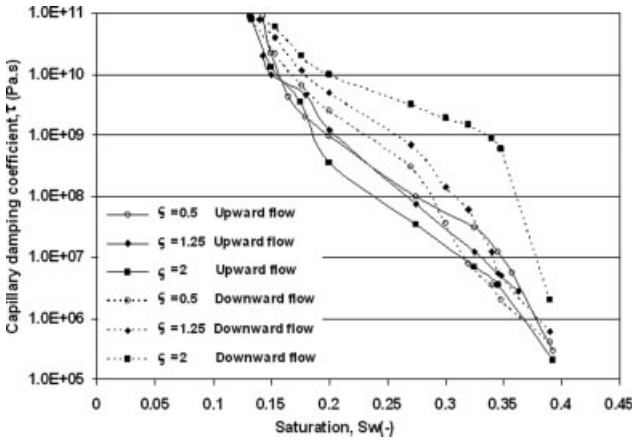

Figure 13. Capillary damping coefficient (τ) for varying density ratio ($\varsigma = \rho_{nw}/\rho_w$) in fine sand cylindrical domain (3D) with flow of PCE downward along gravity and upward against gravity.

linear dynamic P^c relationship (Eq. 1) as the aqueous saturation decreases. The point at which the transition from nonlinear to linear functional form takes place (as shown in Figure 3) seems to depend upon the nonwetting fluid used.[2,13] This suggests again that at higher wetting phase saturation the dynamic capillary relationship is not necessarily the most accurate form. The correlation of τ to the stability of the invading front is evident in case of all silicone oils, as illustrated in Figures 15a,b. In both figures, the average water saturation in the domain is 0.3; however, the saturation distribution is different depending on fluid properties. Figure 15a shows a relatively stable invading front for downward flow of Oil 4 at $S_w = 0.3$. This is an LNAPL of high viscosity ($\mu = 487$ cp) and corresponds to a low value of τ. In this case both viscous and buoyancy forces are highly favourable to a stable front. Figure 15b shows a less stable front for the downward flow of Oil 1, which is an LNAPL of low viscosity ($\mu = 0.49$ cp). This corresponds to higher values of τ (Figure 14).

Further discussions and conclusions

In this work, continuum scale simulations have been carried out to quantify the effects of fluid properties on dynamic capillary pressure for two-phase flow in cylindrical porous media (3D). The simulated data have been fitted to a linear relationship for dynamic capillary pressure,[1] which provides the values of a dynamic coefficient, τ. τ indicates the speed/ease with which a fluid–fluid interfaces may reach equilibrium positions at a given saturation. The determination of realistic values of τ is particularly important to apply the dynamic capillary pressure theories in practice. The effects of fluid properties on τ have not very well characterized in the existing literature. We therefore expect that the results presented in this article will serve to eliminate some of the uncertainties that exist at the moment regarding the range of τ values. The dynamic coefficients found in this work are nonlinear functions of saturation, increasing for decreasing aqueous saturation. This is contrary to results of Stauffer[8] (Eq. 2), which suggest that τ is independent of saturation. However our results are consistent with most recent studies.[2,15] The linear dynamic capillary pressure relationship of Hassanizadeh and Gray[1] is generally found to be valid for a range of saturations if an intercept parameter is included in the original formulation.

The drainage simulations carried out for varying viscosity ratios (μ_{nw}/μ_w) show a decrease in the dynamic coefficient for increasing nonwetting fluid viscosity (μ_{nw}). This is thought to be a consequence of the change in stability of the invading nonwetting fluid front. The stability of the fluid fronts is indicated in this work by the calculation of a mobility coefficient ($m = K_{rw}\mu_{nw}/K_{rnw}\mu_w$), which correlates to τ. At a given saturation for drainage, a larger mobility coefficient describes a more stable front and correlates to a lower value of τ, and vice versa. Simulations carried out for varying density ratios (ρ_{nw}/ρ_w) and infiltration directions show an increase in τ for infiltration directions in which buoyancy forces are favourable and a decrease in τ for infiltration in directions against buoyancy forces. This is again explained in terms of the stability of the fluid flow front. Buoyancy forces in the direction of flow impart instability to the front and buoyancy forces against the direction of flow stabilize the front. These result in higher and lower values of the capillary damping coefficient, respectively.

The studies so far (including this work) show that the dynamic effect is a result of not only the applied boundary pressure but also the material and fluid properties. As discussed in the introduction of this article, roles of a number of material parameters have been discussed in the literature. In this article, we consider the effects of fluid properties on τ. In all our simulations, we use realistic properties of the porous domain and fluids. The fluid properties have been chosen which are relevant from the viewpoints of environmental pollution. Stauffer[8] suggested that the size of dynamic effect depends on the porosity and length of porous media but independent of saturation. Stauffer's scaling relationship also sug-

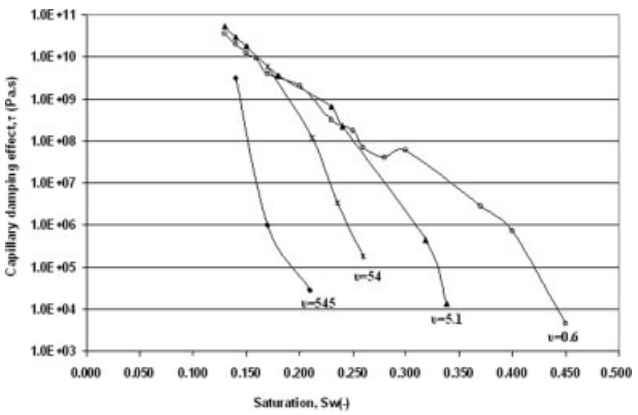

Figure 14. Capillary damping coefficient (τ) for various silicone oils in Table 2. Oils are distinguished by their viscosity ratio ($\upsilon = \mu_{nw}/\mu_w$) in the table.

Although the dynamic coefficient here is a result of the lumped effect of various fluid properties in Table 2, the density ratios in various oils are not significantly different.

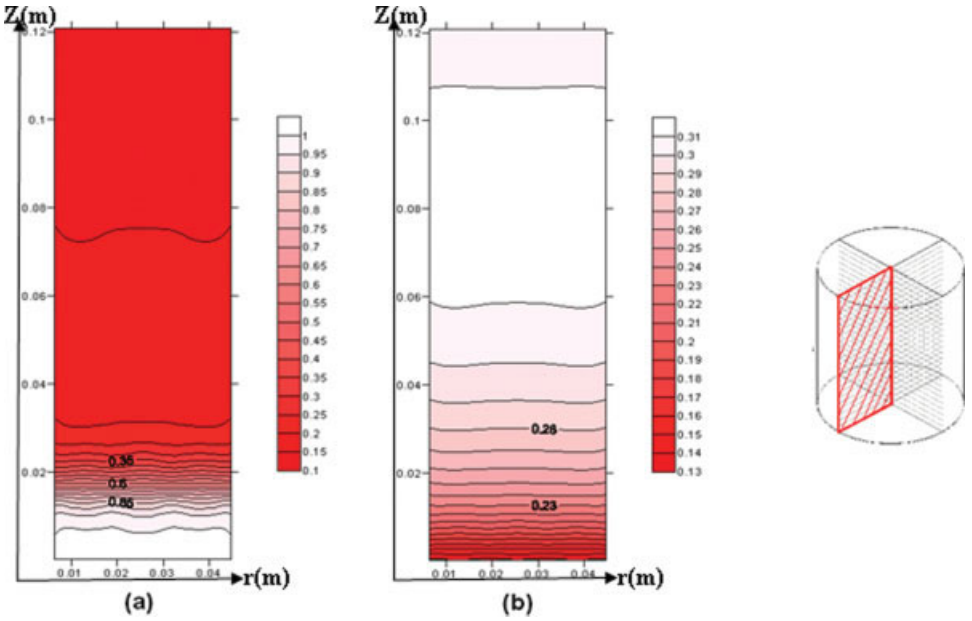

Figure 15. NAPL saturation contour plots for silicone oils (Table 2) on a symmetrical section (12 cm height × 6 cm width) of the cylindrical domain (shown on the right) in downward flow direction: (a) reference Oil 4 with high viscosity and (b) Oil 1 with low viscosity.

In both cases the mean saturation in the domain is 0.3 and the considered NAPL head is 100 cm. [Color figure can be viewed in the online issue, which is available at www.interscience.wiley.com.]

gests that for porous domain with high entry pressure or low permeability, the dynamic coefficient is larger. Mirzaei and Das[2] demonstrated that the dynamic effect depends on aspect ratio (L/D) or sample volume (V) and media permeability. The results presented in this article show that the directions of flow and gravity affect the size of dynamic effect. From the parameters identified so far, it seems therefore that τ [$ML^{-1}T^{-1}$] is a function of wetting phase saturation, S_w [−]; pore size distribution index, λ [−]; porous medium entry pressure, P^d [$ML^{-1}T^{-2}$]; porosity, ϕ [−]; permeability [L^2]; volume of the domain, V [L^3]; fluids density ratio, $\varsigma = \rho_{nw}/\rho_w$ [−], fluids viscosity ratio, $\upsilon = \mu_{nw}/\mu_w$ [−] and, gravity, g [LT^{-2}]. Hence, one may argue that a functional relationship for τ in terms of media and fluid properties can be obtained to generalize their effects. It seems to us that the above variables can be combined into a functional form by applying the Buckingham Π-theorem for dimensional analysis[3,37], i.e.,

$$\mathrm{f}\left(\underbrace{\tau}_{\text{dependent variable}};\underbrace{\phi, P^{\mathrm{d}}, \lambda, K, V, \varsigma, \upsilon, g, S_{\mathrm{w}}}_{\text{independent variables}}\right) = 0 \qquad (18)$$

For our dimensional analysis, τ is defined as the dependent variable while the remaining parameters are assumed to be independent so that there is no correlation among them. By using the Buckingham Π-theorem, the above functional dependence can then be reduced to,

$$\frac{\tau\sqrt{g}}{P^{\mathrm{d}}V^{1/6}} = \mathrm{f}\left(\frac{\phi}{\lambda}, \frac{\varsigma}{\upsilon}, \frac{\mathrm{K}}{V^{2/3}}, S_{\mathrm{w}}\right) \qquad (19)$$

Equation 19 suggests that it may be possible to obtain a functional dependency of τ on different variables. The left hand side of the equation is the dimensionless τ. If derived, scaling relationships such as shown in Eq. 19 can be very cost-effective in terms of simulation time to determine τ–S relationships for real life problems at various scales of observations. In practice, however, it is not trivial to obtain the general solutions to these relationships, their range of validity and the significant groups of variables or parameters as τ depends on a very complex interplay of variables. We believe these relationships are best established by a detailed set of analytical and experimental studies for specific fluid and material properties which are beyond the scope of this article. Nevertheless, we have carried out regression analyses of our simulated results for given ϕ, λ, K, V, and pair of fluids, PCE and water (i.e., known ς and υ) to identify the functional dependence of dynamic coefficient. Following the procedures of Buckingham Π-theorem, it seems that Eq. 19 can be rewritten as below while maintaining the dimensional consistency of the relationship,

$$\tau = C\frac{P^{\mathrm{d}}V^{1/6}}{\sqrt{g}}\left(\frac{\phi}{\lambda}\times\frac{\varsigma}{\upsilon}\right)^{\mathrm{a}}\left(\frac{K}{V^{2/3}}\right)^{\mathrm{b}}(S_w)^{c}; \quad \varsigma = \frac{\rho_{\mathrm{nw}}}{\rho_{\mathrm{w}}}; \quad \upsilon = \frac{\mu_{\mathrm{nw}}}{\mu_{\mathrm{w}}} \qquad (20)$$

where C is a dimensionless constant of proportionality and, $\mathrm{a} = \mathrm{f}(K/V^{2/3})$, $\mathrm{b} = \mathrm{f}(S_w)$, and c are dimensionless coefficients. Equation 20 is a scaling relationship which shows that for given fluid and material properties the dynamic coefficient varies according to S_w and size/volume of the sample (V). The coefficients C, a, b, c must be obtained for individual scenario separately. For example, in case of downward PCE flow (along

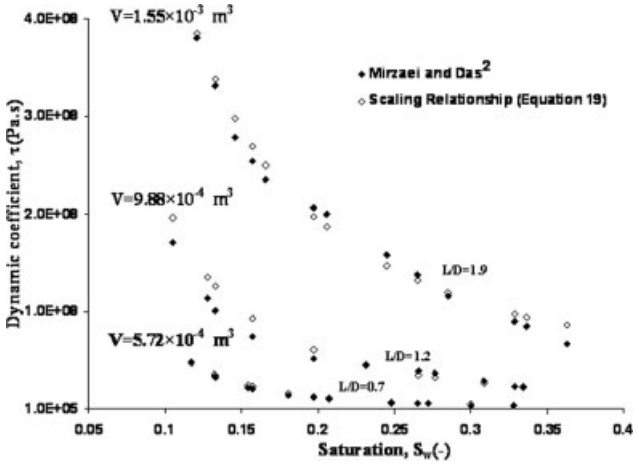

Figure 16. Comparison of τ–S relationships predicted from using Eqs. 20 and 21 and by Mirzaei and Das[2] for different volumes (V) domain (3D) for PCE flow in coarse sand (Table 1).

All domains are cylindrical in shape and their volume (V) is determined by aspect ratio defined as the ratio of length (L) to the diameter (D) of the domain.

gravity) in 3D coarse sand domain (Table 1), these coefficients are as follows,

$$\left.\begin{aligned} C &= 1 \\ a &= 50.195\times\left(\frac{K}{V^{2/3}}\right)^{-0.0029} \\ b &= -1.6\ln(S_w) - 6.8 \\ c &= -25.5 \end{aligned}\right\} \qquad (21a\text{–}d)$$

In Figure 16, we show how the τ–S_w relationships predicted from Eq. 20 for parameters in Eq. 21 compare to numerically derived τ–S_w relationships[2] for various size (V) of coarse sand domain (3D). As evident, the figure indicates excellent comparisons of the τ–S_w relationships from the two cases. Such scaling relationships may be obtained in various scenarios including heterogeneous domain. However, they are outside the scope of this study and not attempted.

Acknowledgments

This study has been carried in the framework of the EPSRC (UK) Project GR/S94315/01, "micro-heterogeneity and temperature effects on dynamic capillary pressure-saturation relationships for two-phase flow in porous media." The EPSRC funding is gratefully acknowledged. Comments of the referees are acknowledged which helped to improve the content of the article.

Literature Cited

1. Hassanizadeh SM, Gray WG. Thermodynamic basis of capillary pressure in porous media. *Water Resour Res*. 1993;29:3389–3405.
2. Mirzaei M, Das DB. Dynamic effects in capillary pressure-saturations relationships for two-phase flow in 3D porous media: implications of micro-heterogeneities. *Chem Eng Sci*. 2007;62:1927–1947.
3. Collins RE. *Flow of Fluids through Porous Materials*. USA: Reinhold Publishing, 1961.
4. Brooks RH, Corey AT. *Hydraulic Properties of Porous Media. Hydrology Papers*. Fort Collins, CO: Colorado State University, 1964.
5. Van Genuchten MT. A closed-form equation for predicting the hydraulic conductivity of unsaturated soils. *Soil Sci Am J*. 1980;44: 892–898.
6. Bear J, Verruijt A. *Modeling Groundwater Flow and Pollution, Theory and Applications of Transport in Porous Media*. Boston, MA: Reidel, 1987.
7. Helmig R. *Multiphase Flow and Transport Processes in the Subsurface*. Heidelberg-Berlin: Springer Verlag, 1997.
8. Stauffer F. Time dependence of the relationship between capillary pressure, water content and conductivity during drainage of porous media. In proceedings of the IAHR conference on scale effects in porous media, Thessaloniki, Greece, 1978.
9. Bourgeat M, Panfilov E. Effective two-phase flow through highly heterogeneous porous media: capillary nonequilibrium effects. *Comput Geosci*. 1998;2:191–215.
10. Ioannidis MA, Chatzis I, Lemaire C, Perunarkilli R. Unsaturated hydraulic conductivity from nuclear magnetic resonance measurements. *Water Resour Res*. 2006;42:W07201, doi:10.1029/2006WR004955.
11. Ioannidis MA, Chatzis I, Dullien, FAL. Macroscopic percolation model of immiscible displacement: effects of buoyancy and spatial structure. *Water Resour Res*. 1996;32:3297–3310.
12. Das DB, Hassanizadeh SM. *Upscaling Multiphase Flow in Porous Media: From Pore to Core and Beyond*. Dordrecht, The Netherlands: Springer Verlag, 2005:1–3, ISBN: 1-4020-3513-6.
13. Das DB, Mirzaei M, Widdows N. Non-uniqueness in capillary pressure–saturation-relative permeability relationships for two-phase flow in porous media: implications of intensity and random distribution of micro-heterogeneity. *Chem Eng Sci*. 2006;61:6786–6803.
14. Das DB, Hassanizadeh SM, Rotter BE, Ataie-Ashtiani B. A numerical study of micro-heterogeneity effects on upscaled properties of two-phase flow in porous media. *Trans Porous Media*. 2004;56:329–350.
15. Hassanizadeh SM, Celia MA, Dahle HK. Dynamic effect in the capillary pressure–saturation and its impact on unsaturated flow. *Vadose Zone J*. 2002;1:38–57.
16. Gielen TWJ, Hassanizadeh SM, Nordhaug HF, Leijnse A. Dynamic effects in multiphase flow: a pore-scale network approach. In: Das DB, Hassanizadeh SM, editors. *Upscaling Multiphase Flow in Porous Media: From Pore to Core and Beyond*. Part II, pp. 217–236, Dordrecht, The Netherlands: Springer, 2005. ISBN: 1-4020-3513-6.
17. Dahle HK, Celia MA, Hassanizadeh SM. Bundle-of-tubes model for calculating dynamic effects in the capillary pressure–saturation relationship. *Trans Porous Media*. 2005;58:5–22.
18. Manthey S, Hassanizadeh SM, Helmig R. Macro-scale dynamic effects in homogeneous and heterogeneous porous media. *Trans Porous Media*. 2005;58:121–145.
19. O'Carroll DM, Phelan TJ, Abriola LM. Exploring dynamic effects in capillary pressure in multistep outflow experiments. *Water Resour Res*. 2005;41:W11419, doi: 10.1029/2005WR004010.
20. Oung O, Hassanizadeh SM, Bezuijen A. Two-phase flow experiments in a geocentrifuge and the significance of dynamic capillary pressure effect. *J Porous Media*. 2005;8:247–257.
21. Barenblatt GI, Entov VM, Ryzhik VM. *Theory of Fluid Flows Through Natural Rocks*. Dordrecht, The Netherlands: Kluwer, 1990.
22. Blunt MJ, King P. Relative permeabilities from 2-dimensional and 3-dimensional pore scale network modelling. *Trans Porous Media*. 1991;6:407–433.
23. Nordhaug HF, Celia M, Dahle HK. A pore network model for calculation of interfacial velocities. *Adv Water Resour*. 2003;26:1061–1074.
24. Panfilov M, Panfilova I. Phenomenological meniscus model for two-phase flows in porous media. *Trans Porous Media*. 2005;58:87–119.
25. Whitaker S. Flow in porous media I: A theoretical derivation of Darcy's law. *Trans Porous Media*. 1986;1:3–25.
26. Tsakiroglou CD, Theodoropoulou MA, Karoutsos V. Nonequilibrium capillary pressure and relative permeability curves of porous media. *AIChE J*. 2003;49:2472–2486.
27. Gielen TWJ. Dynamic effects in two-phase flow in porous media: a pre scale network approach. PhD thesis, Delft University of Technology, Delft, The Netherlands, 2007.
28. Singh M, Mohanty KK. Dynamic modelling of drainage through three-dimensional porous materials. *Chem Eng Sci*. 2003;58(1):1–18.
29. Weitz DA, Stokes JP, Ball RC, Kushnick AP. Dynamic capillary pressure in porous media: origin of the viscous-fingering length scale. *Phys Rev Lett*. 1987;59:2967–2970.
30. Oostrom M, Lenhard J. Comparison of relative permeability–saturation–pressure parametric models for infiltration and redistribution of a light nonaqueous phase liquid in sandy porous media. *Adv Water Resour*. 1998;21:145–157.

31. Schroth MH, Istok JD, Selker JS, Oostrom M, White MD. Multifluid flow in bedded porous media: laboratory experiments and numerical simulations. *Adv Water Resour*. 1998;22:169–183.
32. Ataie-Ashtiani B, Hassanizadeh SM, Celia MA. Effects of heterogeneities on capillary pressure–saturation relative permeability relationships. *J Contam Hydrol*. 2002;56:175–192.
33. Ataie-Ashtiani B, Hassanizadeh SM, Oostrom M, Celia MA, White MD. Effective parameters for two-phase flow in a porous medium with periodic heterogeneities. *J Contam Hydrol*. 2001;49:87–109.
34. Patankar SV. *Numerical Heat Transfer and Fluid Flow*. New York: Hemisphere, 1980.
35. Versteeg HK, Malalasekera W. *An Introduction to Computational Fluid Dynamics: The Finite Volume Method*. Harlow, UK: Longman, 1995.
36. Kueper BH, Frind EO. An overview of immiscible fingering in porous media. *J Contam Hydrol*. 1989;5:83–95.
37. Bird RB, Stewart WE, Lightfoot EN. *Transport Phenomena*. New York: Wiley, 1960.

Appendix

Criterion for analyzing effects of fluid properties on dynamic coefficient τ (simplified case)

In this article, we argue that the roles of fluid properties are such that they affect the stability of fluid–fluid interfaces and consequently the dynamic coefficient, τ. The purpose of Appendix 1 is to derive a simple criterion to explain how various parameters may affect the stability of fluid fronts. Although we carry out 2D or 3D simulations, the criterion is derived for 1D as it simplifies the analysis. However, the conclusions are general enough that they can be adapted for 2D/3D simulations. For our purpose, we consider drainage of a porous material placed in a pressure cell, as shown in Figure A1. It is assumed that for any reason a bump (e.g., finger) of arbitrary size ε is produced as the fluid front moves through the domain. The fluid–fluid interface is defined to be at $x = X_f$. For simplicity we also assume that in the region $0 < x < X_f$, the domain is at irreducible water saturation, S_{rw}, while in the region $X_f < x < X$ the domain is fully saturated with water (Figure A1). For generality of the approach, the domain and the flow direction are defined to be at an angle θ above the horizontal so that for downward flow along gravity, upward flow against gravity and horizontal, $\sin\theta = -1, 1, 0$, respectively.

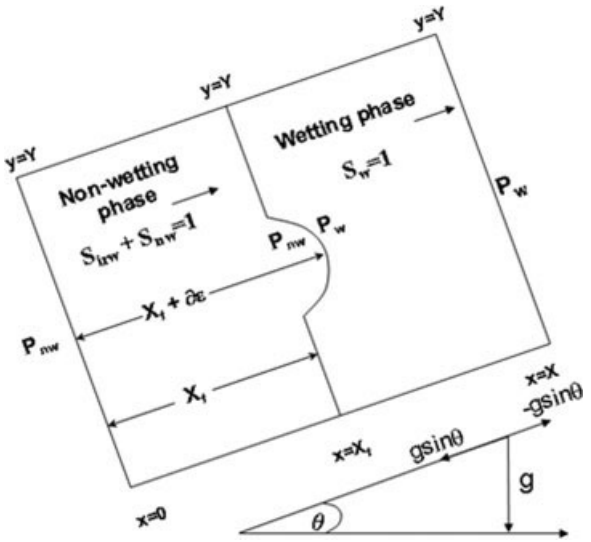

Figure A1. A schematic for drainage of porous media in a pressure cell on the horizontal plane (*x–y*).

At certain time (t) and average domain water saturation (S_w), the pressure distributions of the fluid phases in the domain are obtained from Darcy's equation (Eq. 5):

$$\frac{\partial^2 P_{nw}}{\partial x^2} = 0 \quad \text{for} \quad 0<x<X_f; \frac{\partial^2 P_w}{\partial x^2} = 0 \quad \text{for} \quad X_f<x$$

Subject to the following boundary conditions (BCs):

$$P_{nw} = P_1 \quad \text{at} \quad x = 0; \quad P_w = P_2 \quad \text{at} \quad x = X \qquad \text{(A.3–4)}$$

So that, $\Delta P = P_1 - P_2$. Integrating Eqs. A.1 and A.2,

$$P_{nw} = Ax + B; \quad P_w = Cx + D \qquad \text{(A.5–6)}$$

where A, B, C, D are constants of integration. Differentiating Eqs. A.5–6 with respect to x, we obtain,

$$\frac{\partial P_{nw}}{\partial x} = A \quad ; \quad \frac{\partial P_w}{\partial x} = C \qquad \text{(A.7–8)}$$

If the pressures of the wetting and nonwetting phases are $P_{w,f}$ and $P_{nw,f}$ across the fluid–fluid interface at $x = X_f$, then the interface capillary pressure is,

$$P_f^c = P_{nw,f} - P_{w,f} \quad \text{or} \quad P_{nw,f} = P_f^c + P_{w,f} \quad \text{at} \quad x = X_f \qquad \text{(A.9)}$$

We define that the Darcy fluxes of the nonwetting (q_{nw}) and wetting (q_w) phases per unit area normal to the fluid–fluid interface are the same, such that,

$$\frac{K_{rnw}}{\mu_{nw}}\left[\frac{\partial P_{nw}}{\partial x} + \rho_{nw} g \sin\theta\right] = \frac{K_{rw}}{\mu_w}\left[\frac{\partial P_w}{\partial x} + \rho_w g \sin\theta\right] \qquad \text{(A.10)}$$

Or,

$$A + \rho_{nw} g \sin\theta = m[C + \rho_w g \sin\theta]$$

$$\text{where m} = \frac{K_{rw}\mu_{nw}}{K_{rnw}\mu_w} \text{ is the mobility ratio/coefficient} \qquad \text{(A.11)}$$

Solving for the constants in Eqs. A.5–6, we find that,

$$A = -\frac{m\Delta P - (m\rho_w - \rho_{nw})(X - X_f) g \sin\theta - mP_f^c}{X + X_f(m-1)} \qquad \text{(A.12)}$$

$$B = P_1 \qquad \text{(A.13)}$$

$$C = -\frac{\Delta P + (m\rho_w - \rho_{nw}) X_f g \sin\theta - P_f^c}{X + X_f(m-1)} \qquad \text{(A.14)}$$

$$D = P_2 + \frac{\Delta P + X_f(m\rho_w - \rho_{nw}) g \sin\theta - P_f^c}{X + X_f(m-1)} X \qquad \text{(A.15)}$$

Assuming that the fluid–fluid interface moves a distance δX_f over a time period δt at a uniform speed v_f, we have $v_f = \frac{\delta X_f}{\delta t}$. Now, carrying out a mass balance for water flow

over unit area for the time duration δt, $q_{\mathrm{nw}}\delta t = \phi\delta X_{\mathrm{f}}(1 - S_{\mathrm{rw}})$, where S_{rw} is the irreducible water saturation of the porous domain. From this it follows that,

$$\frac{\delta X_{\mathrm{f}}}{\delta t} = \frac{m}{\phi(1 - S_{\mathrm{rw}})}\frac{K_{\mathrm{nrw}}}{\mu_{\mathrm{nw}}} \times \left[\frac{\Delta P - X\rho_w g\sin\theta + X_f\rho_w g\sin\theta - X_f\rho_{nw}g\sin\theta - P_f^c}{X + X_f(m-1)}\right]$$

However, the speed of fluid interface at the tip of the bump is,

$$\frac{\delta(X_{\mathrm{f}}+\varepsilon)}{\delta t} = \frac{m}{\phi(1-S_{\mathrm{rw}})}\frac{K_{\mathrm{nrw}}}{\mu_{\mathrm{nw}}} \times \left[\frac{\Delta P - X\rho_{\mathrm{w}}g\sin\theta + (X_{\mathrm{f}}+\varepsilon)\rho_{\mathrm{w}}g\sin\theta - (X_{\mathrm{f}}+\varepsilon)\rho_{\mathrm{nw}}g\sin\theta - P_{\mathrm{f}}^{\mathrm{c}}}{X + (X_{\mathrm{f}}+\varepsilon)(m-1)}\right]$$

Thus, the rate of change of the bump size at a given average saturation is,

$$\frac{\delta\varepsilon}{\delta t} = -\frac{\varepsilon m(m-1)}{\phi(1-S_{\mathrm{rw}})}\frac{K_{\mathrm{nrw}}}{\mu_{\mathrm{nw}}} \times \frac{\Delta P - \left[(X_{\mathrm{f}}+\varepsilon)\left(\frac{\rho_{\mathrm{nw}}}{\rho_{\mathrm{w}}} - 1\right) + X\right]\rho_{\mathrm{w}}g\sin\theta - P_{\mathrm{f}}^{\mathrm{c}}}{[X + (X_{\mathrm{f}}+\varepsilon)(m-1)][X + X_{\mathrm{f}}(m-1)]}$$

Or,

$$\frac{\delta\varepsilon}{\delta t} = -\frac{\varepsilon m(m-1)}{\phi(1-S_{\mathrm{rw}})}\frac{K_{\mathrm{nrw}}}{\mu_{\mathrm{nw}}} \times \frac{\Delta P - \left[X_{\mathrm{f}}\left(\frac{\rho_{\mathrm{nw}}}{\rho_{\mathrm{w}}} - 1\right) + X\right]\rho_{\mathrm{w}}g\sin\theta - P_{\mathrm{f}}^{\mathrm{c}}}{[X + X_{\mathrm{f}}(m-1)]^2}\ ;\quad X_{\mathrm{f}} >> \varepsilon \quad \text{(A.16)}$$

In the absence of gravity forces and capillary pressure at fluid/fluid interfaces we have,

$$\frac{\delta\varepsilon}{\delta t} = -\frac{\varepsilon m(m-1)}{\phi(1-S_{\mathrm{rw}})}\frac{K_{\mathrm{nrw}}}{\mu_{\mathrm{nw}}}\frac{\Delta P}{[X + X_{\mathrm{f}}(m-1)]^2} \qquad \text{(A.17)}$$

Equation A.17 suggests that the size (ε) of the bump (e.g., finger) decays or grows with time depending on whether $m > 1$ or $m < 1$, respectively. In general, higher is the value of m the more stable the fluid front is. For the purpose of this article, we argue that increase in the bump size with time indicates instability of flow, and vice versa. For stable flow, the relaxation parameter (τ) should be low, i.e., higher is the value of m, the smaller is the value of τ. Inclusion of capillary pressure at the fluid–fluid interface $\left(P_{\mathrm{f}}^{c}\right)$ stabilizes the front (Eq. A.16) provided all other parameters remain the same and $P_{\mathrm{f}}^{\mathrm{c}}$ is positive. In other words, τ is smaller in this case as compared to the situations where $P_{\mathrm{f}}^{\mathrm{c}}$ is less, ignored, or negative. The effects of gravity on $\delta\varepsilon/\delta t$ depend on the density ratio $(\rho_{\mathrm{nw}}/\rho_{\mathrm{w}})$ and directions of flow, i.e., the value of g sin θ, θ being the angle of flow above the horizontal. For example in case of DNAPL $[\rho_{\mathrm{nw}}/\rho_{\mathrm{w}} > 1]$, downward flow (sin θ = −1) imparts additional instability to the invading front (Eq. A.16) and thus τ is higher as compared with those cases where gravity is ignored. For flow against gravity (sin θ = 1), a DNAPL front is more stable and therefore τ is lower. For the horizontal flow gravity has no affect on stability of the front (sin θ = 0) and therefore τ values for this case lie between the cases for upward and downward flow. We provide quantitative supports for some of these arguments/hypotheses through the results of our 3D numerical simulations of two-phase flow in porous medium where all effects of m, $P_{\mathrm{f}}^{\mathrm{c}}$, and g sin θ are lumped in the τ–S relationships.

Manuscript received Feb. 28, 2007, and revision received July 25, 2007.